Coherent Control of the Energy and Angular Distribution of Autoionized Electrons

R. van Leeuwen, M. L. Bajema, and R. R. Jones
Department of Physics, University of Virginia, Charlottesville, Virginia 22901
(Received 31 July 1998)

Nonstationary, autoionizing wave packets have been produced by exposing calcium Rydberg atoms to a pair of identical phase-coherent subpicosecond laser pulses. The energy and angular distribution and time of ejection of electrons has been altered by changing the relative phase and delay between the two laser pulses. [S0031-9007(99)08888-2]

PACS numbers: 32.80.Rm, 33.80.Rv

Optical control over the branching ratio for nonradiative decay of excited states of atoms and molecules is an ongoing problem in physics [1], and several methods for manipulating the relative yield into a number of energetically flat, unstructured continua have been proposed [2–4]. In the frequency domain, differential control has been achieved by exploiting quantum mechanical interference between multiple excitation paths into the continua [5–7] and laser-induced continuum structure (LICS) [8]. Typically, these schemes require light at two different frequencies, and the experimental "knob" that enables branching ratio manipulation is either the relative optical phase between the two laser pulses [6,7] or the detuning of one laser from a bound or quasibound resonance [5,8]. In the time domain, reaction product control has been realized through the application of sequences of ultrashort, time-delayed laser pulses [9]. In its simplest form, one laser pulse creates a nonstationary wave packet that moves about the potential energy surface accessing different allowed configurations. A second, time-delayed pulse is then used to selectively excite the wave packet into a particular continuum mode at a specific time [2].

While these methods enable control of differential processes through flat continua, most multiconfigurational systems of interest have intrinsic continuum structure. It is well known that continuum resonances provide a mechanism for altering product branching ratios as a function of the frequency of a single exciting laser pulse [8,10]. Furthermore, since the presence of resonances often enhances the total process yield, the importance of continuum structure on optical control experiments is well established, at least in the frequency domain [6,7,11]. However, continuum-resonance facilitated control has yet to be demonstrated in the time domain, where one can modify the time dependence of the emission into various continuum channels as well as the total branching ratio for the process.

In this Letter, we present an experimental demonstration of differential process control in the time domain using two identical laser pulses to coherently excite a structured, multiconfigurational continuum. Specifically, a 0.4 psec laser pulse photoexcites $4sns\,^1S_0$ calcium Rydberg atoms to an energy just below the $Ca^+ 4p_{1/2}$ ionization limit. The pulse performs an "isolated core excitation" (ICE) [12], producing a *nonstationary* coherent superposition of dielectronic states in a single bound configuration, $4p_{3/2}nsJ = 1$, at an energy greater than 3 eV above the first ionization limit (see Fig. 1). Because of the repulsive electron-electron Coulomb interaction, the two valence electrons coherently scatter into bound $4p_{1/2}n's$ modes (configuration interaction) as well as $4s_{1/2}\epsilon\ell$ and $3d_{3/2,5/2}\epsilon'\ell'$ continuum channels (autoionization). Autoionization into each available continuum channel occurs directly, through the $4p_{3/2}$ channel, and indirectly, through the $4p_{1/2}$ configuration. Since the bound character of the nonstationary wave packet changes as time evolves [13], the direct and indirect autoionization contributions vary as a function of time [14], and the electrons ejected into each continuum channel experience time-dependent multiple-path interference.

The time dependence of the interference can be exploited to control the energy and angular distributions of the ejected electrons by using a second, identical

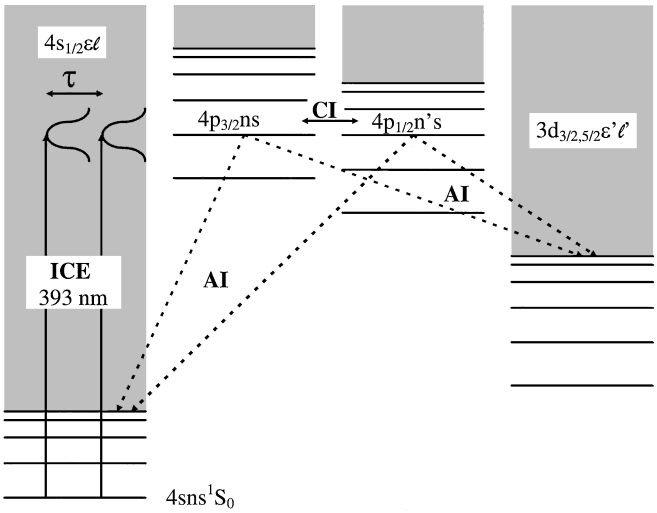

FIG. 1. Schematic energy level diagram of calcium showing the isolated core excitation (ICE) and the relevant bound-bound (configuration interaction denoted by CI) and bound-unbound couplings (autoionization denoted by AI). Five bound and eight continuum channels contribute to the $J = 1$ spectrum at the energies of interest in the experiment.

 0031-9007/99/82(14)/2852(4)$15.00

phase-coherent laser pulse. The second pulse coherently excites additional amplitude into the $4p_{3/2}ns$ configuration which interferes with any amplitude remaining in this initial bound mode [15]. In fact, the second pulse modulates any residual $4p_{3/2}ns$ amplitude as the relative phase (delay) between the two identical pulses is varied, altering the time dependence of the differential autoionization yield. We find that the branching ratio for ejection of electrons into the $4s_{1/2}$ continua can be varied by more than 20%. This control is achieved through multiple sets of interfering pathways that depend on both the relative optical phase and on an intrinsic atomic phase produced by the time-dependent configuration interaction. Although this experiment involves dielectronic states in atoms, the general method is applicable to any multiconfigurational system with continuum structure.

In the experiment, ground state $4s4s^1S_0$ Ca atoms in an effusive atomic beam are resonantly excited to a stationary $4s14s^1S_0$ Rydberg level via a $4s5p^1P_1$ intermediate state. The tunable laser light required for these transitions is generated from the output of two optical parametric amplifiers (OPAs) that are pumped by approximately 90% of the 2.2 W, 787 nm, 100 fs output of a 1 kHz Ti:sapphire regenerative amplifier. The Rydberg atoms are then exposed to a pair of identical 0.4 psec, phase-coherent laser pulses with wavelengths centered at the Ca^+ $4s \rightarrow 4p_{3/2}$ interval at 393 nm. Each pulse has an energy of only a few μJ and drives an ICE to the $4p_{3/2}14s$ $J = 1$ part of a structurally mixed autoionizing resonance [16]. This resonance lies 3.1 eV above the $4s_{1/2}$-ionization limit and 1.5 eV above the $3d_{3/2,5/2}$ limits (see Fig. 1) and contains $4p_{3/2}14s$ and $4p_{1/2}16s$ bound-state character [16]. During the transition, the Rydberg electron acts as a spectator [12], and there is essentially zero direct excitation of the $4s_{1/2}$ or $3d_{3/2,5/2}$ continua. Since the bandwidth of the laser pulses (40 cm^{-1}) is much smaller than the 223 cm^{-1} fine-structure splitting of the Ca^+4p level there is also negligible *direct* excitation of the $4p_{1/2}ns$ $J = 1$ configuration [17].

The two phase-coherent 393 nm (UV) pulses are produced by sending a single parent UV pulse through a Michelson interferometer. The parent pulse is generated by frequency doubling 10% of the 787 nm Ti:sapphire output in a 1-cm-long KDP crystal. The long nonlinear crystal restricts the bandwidth of the UV pulse to 40 cm^{-1} approximately matching the width of the excited autoionizing resonance [16]. The time delay and relative phase between the two pulses is varied by changing the optical path length of one arm of the interferometer using a piezoelectric driven translation stage.

The laser and atomic beams interact between two grounded capacitor plates. A fraction of the electrons that are ejected in the autoionization process pass through a 1 mm diameter hole in one of the plates and are collected by a microchannel plate detector. The electrons emitted into the $4s$ and $3d_j$ continua are distinguished by different flight times to the detector. The fast (3.1 eV) and slow (1.5 eV) electron signals are simultaneously recorded as a function of the delay between the two UV pulses.

Figure 2 shows the yield of slow and fast electrons ejected parallel to the laser polarization (0°) as a function of the time delay between the UV pulses. The modulation in the net autoionization signal in each continuum channel is a reflection of delay dependent interference in the $4p_{3/2}14s$ excitation amplitude [14]. In fact, because the experiment is performed in the "weak-field" limit, the electron signal is simply a constant added to a linear superposition of sine waves [15,18]. Each component sine wave has a frequency within the bandwidth of the UV pulses and the strength of each component is proportional to the excitation cross section multiplied by the laser spectrum [18]. Since any real signal must exhibit oscillations within the laser bandwidth, the data are collected using a software filter that is locked to the translation stage step frequency and rejects any signal variations not at the laser frequency. To ensure that all of the real signal is collected, the bandwidth of the filter is 150 cm^{-1}, nearly four times greater than that of the UV pulses [19]. Each data point in Fig. 2 represents 80 laser shots, and approximately 10 data points are recorded over each interference cycle. The insets in Fig. 2 provide a magnified view of the data at specific delays, clearly showing the rapid interference oscillations.

For small delays, the wave packet produced by the first pulse has not changed significantly when the second pulse arrives. Consequently, the overlap between the wave packets produced by the two pulses is nearly perfect and the interference signal is large. As the relative phase

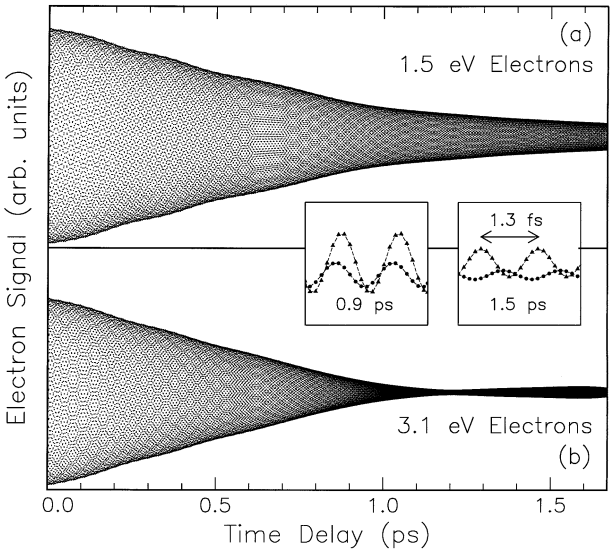

FIG. 2. (a) Slow, 1.5 eV, and (b) fast, 3.1 eV, electron signal versus delay between the two phase-coherent pulses. Only electrons ejected parallel to the laser polarization (0°) are detected. Insets: High resolution view of the rapid oscillations in the slow (solid triangle) and fast (solid circle) electron yield at $\tau = 0.9$ psec and $\tau = 1.5$ psec.

between the two pulses is changed, the electron signal in each continuum varies from zero to four times the yield due to the first pulse alone [15]. For increasing delays, autoionization and configuration interaction reduce the amount of $4p_{3/2}$ character that remains when the second wave packet is produced, decreasing the level of interference between the two packets [14]. At long delays, the first wave packet has completely autoionized before the second laser pulse arrives. Consequently, the wave packets produced with different pulses cannot interfere, and the total signal is equal to twice the single pulse yield. For electrons ejected at 0°, the branching ratio for decay into the $4s$ continuum at large delays is 47% in good agreement with the experimental frequency domain value of 43% at the $4s$-$4p_{3/2}$ ionic transition [16].

The envelope of the slow electron interferogram in Fig. 2a exhibits, primarily, an exponential decay convoluted with the finite duration of the laser pulse. The fast electron interferogram in Fig. 2b shows a qualitatively different behavior. Most notably, its envelope has a node at $\tau \approx 1.2$ psec. The difference in the interferograms stems from the interplay between interferences intrinsic to the autoionization process as well as those due to the coherent pulse excitation process. These differences are reflected in the branching ratio for decay into the respective continuum channels.

The branching ratio, BR, for decay into the fast electron channel is obtained by dividing the signal in Fig. 2b by the sum of the signals in Figs. 2a and 2b. In contrast to the fast and slow electron signals, the temporal modulations in BR are not necessarily sinusoidal, as is shown in the insets of Fig. 3. The thick solid curve in Fig. 3 shows the peak to peak variation in BR for electrons ejected at 0° as a function of delay between the two laser pulses. For delays between 0.6 and 1.4 psec, the variation in BR is greater than 20% due to both amplitude *and* phase differences between the fast and slow electron interferograms.

For delays, $\tau < 1.2$ psec, the time dependence of BR is due primarily to the differences in the envelopes of the interferograms. The bold dashed curve in Fig. 3 shows the variation in BR determined directly from the envelopes of the interferograms in Figs. 2a and 2b. However, the interferograms exhibit a pronounced, delay-dependent "phase lag" [6,7] which contributes significantly to the total control level at large delays. The time dependence of the phase lag is shown explicitly in Fig. 4. At $\tau \approx 1.2$ psec a π phase shift between the fast and slow interference pattern occurs, coinciding with the node in the fast electron interferogram. As a result, at longer delays, the oscillating fast and slow electron signals are almost completely out of phase. Therefore, the peak to peak variation in BR remains significant, even at large delays when the envelopes of both interferograms are essentially constant.

Analogous measurements made for electrons ejected at 90° show that the fast and slow electron interferograms are both very similar to the 0° slow electron interferogram. As a result, the peak to peak variation in the branching ratio is smaller than 5% at all delays, as shown by the thin curves in Fig. 3. No node appears in either interferogram, and the phase difference between the fast and slow electron signal is close to zero at all delays (see the dashed curve in Fig. 4). Since the interferograms for fast electrons ejected at 0° and 90° are quite different, the *angular distribution* of the ejected electrons must also

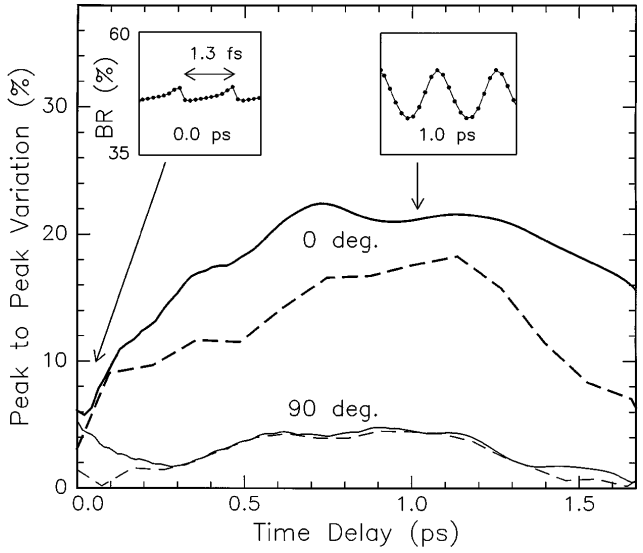

FIG. 3. Peak to peak variation in the branching ratio (BR) for autoionization into the 3.1 eV channel as a function of delay between the two laser pulses. The BR is shown relative to that observed with a single laser pulse for electrons ejected at 0° (bold solid line) and 90° (light solid line). The variation in the BR due to the envelope of the interferograms only is shown by the analogous dashed curves. The insets show the periodic, but nonsinusoidal, variation in the BR at $\tau = 0.0$ psec and $\tau = 1.0$ psec delay.

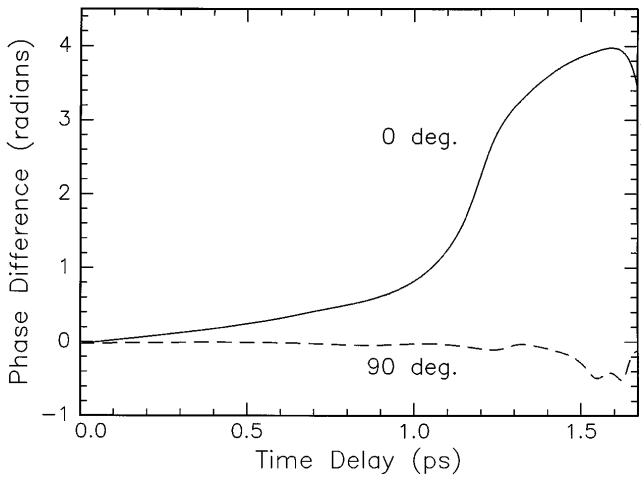

FIG. 4. Phase difference between the rapid oscillations in the fast and slow electron interferograms for ejection at 0° (solid curve) and 90° (dashed curve) as a function of the delay between the two phase-coherent laser pulses.

depend on the delay between the two identical pulses. We have observed similar behavior in excitation from Rydberg states other than $4s14s$ as well.

It is interesting to compare and contrast the role of resonances in our experiment with that in recent $\omega_0 + 3\omega_0$ frequency domain phase-control experiments. The recent observation of a frequency-dependent phase lag in $\omega_0 + 3\omega_0$ branching ratio control has been attributed to the energy dependent modification of the continuum due to Fano resonances [7]. In those experiments, both the continuum and bound configurations are directly accessible from the initial state, and it is possible to change the final state branching ratio for the one or three photon process alone by scanning ω_0 across the Fano profile. Of course, the Fano line shape is a manifestation of the energy-dependent variation of the interference between the direct and indirect paths into the continua [17]. The coherent combination of one and three photon processes provides additional interfering pathways that can be manipulated for additional branching ratio control [6,7].

In the current experiment, there is no direct excitation of the available continua [12]. Instead, the coupling between the available bound channels produces an energy-dependent variation in the total and partial excitation cross section. Our time domain results can be predicted directly from available frequency domain spectra. In fact, the interferogram for autoionization into each continuum is equal to the Fourier transform of the partial cross section for excitation of that continuum as a function of frequency [18], and the *R*-matrix formulation of multichannel quantum defect theory (MQDT) provides a powerful tool for predicting the time-domain interferences [16,20]. The observed temporal variations in the phase lag and envelopes of the interferograms are a reflection of the multiple path interferences (see Fig. 1) in the decay of the initially excited autoionizing state. These same interferences are the source of the spectral structure in the partial cross sections.

It is important to note that the time-domain approach used here allows for control of the *time dependence* of the electron emission into different continua as well as modification of the total branching ratio. This additional "time-of-ejection" control is possible whenever there is significant overlap between resonance structures in the different continua [21], a situation that is realized in our experiment. In our experiment, the emission into one continuum channel has a large amplitude only for small delays while ejection into the other continuum is more probable at longer delays. The application of a second, phase-coherent pulse at intermediate delays can coherently modulate amplitude in the long lived channel only, thereby changing the time dependence of the branching ratio after the second pulse.

In conclusion, we have demonstrated for the first time that configuration interaction between quasibound dielectronic autoionizing states can be exploited to control the energy and angular distribution of ejected electrons in the time domain. The method, which uses two *identical* phase-coherent pulses, can also be used to alter the temporal structure of the differential yield, and is applicable to any multiconfigurational system with structured continua.

We gratefully acknowledge stimulating discussions with T. F. Gallagher and the financial support of the NSF, the UVA AEP, the ONR, and the Packard Foundation.

[1] W. S. Warren, H. Rabitz, and M. Dahleh, Science **259**, 1581 (1993), and references therein.
[2] D. J. Tannor and S. A. Rice, J. Chem. Phys. **83**, 5013 (1985); D. J. Tannor, R. Kosloff, and S. A. Rice, J. Chem. Phys. **85**, 5805 (1986).
[3] S. T. Pratt, J. Chem. Phys. **104**, 5776 (1996).
[4] M. Shapiro, J. W. Hepburn, and P. Brumer, Chem. Phys. Lett. **149**, 451 (1988).
[5] F. Wang, C. Chen, and D. S. Elliott, Phys. Rev. Lett. **77**, 2416 (1996).
[6] L. Zhu *et al.*, Science **270**, 77 (1995).
[7] L. Zhu *et al.*, Phys. Rev. Lett. **79**, 4108 (1997).
[8] A. Shnitman *et al.*, Phys. Rev. Lett. **76**, 2886 (1996); T. Nakajima, J. Zhang, and P. Lambropolous, *ibid.* **79**, 3367 (1997).
[9] J. L. Herek, A. Materny, and A. H. Zewail, Chem. Phys. Lett. **228**, 15 (1994); C. J. Bardeen *et al.*, J. Phys. Chem. A **101**, 3815 (1997); A. Assion *et al.*, Science **282**, 919 (1998).
[10] C. Jungen and D. Dill, J. Chem. Phys. **73**, 3338 (1980); L. D. Van Woerkom and W. E. Cooke, Phys. Rev. Lett. **57**, 1711 (1986).
[11] T. Nakajima, J. Zhang, and P. Lambropolous, J. Phys. B **30**, 1077 (1997).
[12] W. E. Cooke *et al.*, Phys. Rev. Lett. **40**, 178 (1978).
[13] D. W. Schumacher *et al.*, J. Phys. B **29**, L4359 (1996); D. W. Schumacher, B. J. Lyons, and T. F. Gallagher, Phys. Rev. Lett. **78**, 4359 (1997).
[14] M. B. Campbell, T. J. Bensky, and R. R. Jones, Phys. Rev. A **57**, 4616 (1998).
[15] N. F. Scherer *et al.*, Chem. Phys. **93**, 856 (1990); L. D. Noordam, D. I. Duncan, and T. F. Gallagher, Phys. Rev. A **45**, 4734 (1992); R. R. Jones *et al.*, Phys. Rev. Lett. **71**, 2575 (1993).
[16] V. Lange, U. Eichmann, and W. Sandner, J. Phys. B **22**, L245 (1989).
[17] T. F. Gallagher, *Rydberg Atoms* (Cambridge University Press, Cambridge, 1994), 1st ed.
[18] R. R. Jones *et al.*, J. Phys. B **28**, L405 (1995).
[19] Although the constant offset is removed from the data by the filtering procedure the data is restored to its correct form by adding a constant offset which sets the minimum autoionization signal to zero for the first few oscillations near zero delay.
[20] C. H. Greene and L. Kim, Phys. Rev. A **36** 2706 (1987); L. Kim and C. H. Greene Phys. Rev. A **36**, 4272 (1987).
[21] R. van Leeuwen and R. R. Jones (to be published).